Site Response in the Northern San Francisco Bay Area, California

BERGEN, K.J., FLETCHER, J.B., BOATWRIGHT, J., LANGENHEIM, V.E.

DRAFT
02.02.2007

Site Response in the Northern San Francisco Bay Area, California

BERGEN, K.J., FLETCHER, J.B., BOATWRIGHT, J., LANGENHEIM, V., U.S. Geological Survey, Menlo Park, CA 94025, jfletcher@usgs.gov.

Abstract:

Santa Rosa, California sustained unexpectedly high damage from the 1906 San Francisco earthquake (M7.8) and the 1969 Santa Rosa Earthquake sequence (M5.6 and M5.7). At the nearby city of Napa, ground motion was also unexpectedly high during the 2000 Yountville earthquake (M5.2). This history of unexpectedly strong ground motion, in combination with high metropolitan populations in Santa Rosa (over 450,000) and Napa (over 100,000), and their close proximities to Holocene active faults such as the Rodgers-Healdsburg fault system, West Napa Fault, and Green Valley fault, make estimation of site response in these regions particularly important. We estimate site response at 24 sites in this region by inverting seismograms of local events (radius < 100km) for source, site, and propagation characteristics. Regional seismicity was recorded from January, 2004, to September, 2006. We inverted spectra of 33 earthquakes for P-waves and 25 earthquakes for S-waves, covering a range of hypocentral distances and azimuths. Seismic cone penetration testing (SCPT) was done at three stations in Santa Rosa and three stations in Napa to determine near surface S-wave velocities and constrain absolute site amplification. High site response is estimated from the inversion in the city of Napa, in agreement with slower near-surface S-wave velocities from SCPT. Response is estimated to be lower at adjacent sites outside of the valley. Site response is also high in the city of Santa Rosa, although lower than Napa. High response in Santa Rosa is in agreement with faster near-surface S-wave velocities from SCPT.

1. Introduction

Despite the Northern San Francisco Bay region's long history of damage from earthquakes, little work has been done to understand the amplification of seismic waves in this rapidly growing region. Major cities such as Santa Rosa, Petaluma, and Napa have been rapidly growing, with Santa Rosa-Petaluma having a metropolitan population exceeding 450,000 and Napa exceeding 100,000 from 2005 U.S. census figures. Holocene active faults such as the Rodgers Creek-Healdsburg, Green Valley, and West Napa faults bound the sedimentary basins underlying the Santa Rosa Plain, Sonoma Valley, and Napa Valley. Loss estimates from the California Geological Survey for a magnitude 7.0 earthquake on the Rodgers Creek Fault total $8 billion in damage, and estimates for a magnitude 6.5 rupture of the Southern and Northern Green Valley Fault total $3.2 billion (2006). The probabilistic seismic hazard map for the state of California (Peterson et al., 1996) suggests the potential for a magnitude 6.5 earthquake on the West Napa Fault, and Langenheim et al., 2006 suggest even higher magnitudes (M 6.8-7.1) based on length magnitude relations. Furthermore, the rupture probability for a Hayward/Rodgers Creek earthquake is 27% for the period between 2002-2031, the highest of any faults in the San Francisco Bay area (Working Group on California Earthquake Probabilities [WGCEP], 2003).

To achieve a better understanding of these hazards, we deployed an array to determine site response. Seismograms of local earthquakes, recorded from 2004 to 2007, were inverted for source, site, and propagation characteristics. We utilized an existing thirteen-station intermediate period seismic array, and augmented it with a six station array across Santa Rosa and a five station array across the city of Napa to provide more

detailed results for these highly populated areas. We estimate the site-response

characteristics of 24 sites in the Northern Bay for P-waves, and 22 for S-waves. The

earthquakes cover a range of hypocentral distances (6 km $< r <$ 100 km) and azimuths.

We utilize the inversion method outlined in Boatwright et al. (1991) with two different

attenuation models: model tertio estimates a frequency independent mid-crustal Q, and

models and falloff from geometrical spreading as r^{-1}; model tertio(f) estimates frequency

dependent mid-crustal Q by determining Q_0 in the equation $Q(f) = Q_0 f^{0.6}$ and models

falloff from geometrical spreading as r^{-1} for $r <$ 30 km and $r^{-0.7}$ for r $>$ 30 km. Both

inversion techniques estimate the near surface attenuation parameter t^*. We utilize two

datasets for P and S waves with hypocentral radius limits of 55 km and 100 km for

comparison.

In this paper we will outline the historical seismicity, regional geology,

quaternary geology, fault structure, and basin structure of the Northern San Francisco

Bay region. We will discuss the data and methods used in our estimations of site

response spectra and attenuation parameters. Finally we will discuss the results of our

inversions in terms of the basin structure and near-surface geology to try to understand

the mechanisms behind the high shaking intensities observed historically, and in this

study, in the Northern San Francisco Bay region.

2. Historical Seismicity

Several earthquakes larger than magnitude 5 have affected the northern San

Francisco Bay region since 1800. At least five events affected the region prior to the

1906 San Francisco Earthquake. In 1855, an event apparently centered near the San

4

Pablo Bay shoreline in Sonoma County is suggested to have caused Modified Mercali Intensity of shaking (MM) VI based on damage reports of cracked buildings near Petaluma (Toppozada, 2002). Two events in March, 1865, of estimated magnitude 5.2 and 5.1 occurred approximately 6.5 hours apart near Santa Rosa, possibly on the Rodgers Creek-Healdsburg fault zone (Toppozada, 2002). The cities of Napa and Sonoma were significantly shaken (MM VIII) by an earthquake in 1891, damaging windows and chimneys, and knocking down plaster (Toppozada, 2002). An 1893 event with local magnitude (M_L) 5 and MM VII knocked down chimneys and plaster in Santa Rosa (Wong and Bott, 1995). The 31 March 1898 earthquake, suggested to be on the southern Rodgers Creek fault and as large as M_L 6.7 (MM VIII) by Toppozada et al. (1992), collapsed and damaged several buildings on Mare and Tubb Islands and in the city of Napa.

The 1906 San Francisco earthquake (M_w 7.8) and subsequent fire largely destroyed downtown Santa Rosa. Ground motions in Santa Rosa have been estimated to be MM 9-10 from Lawson's 1908 report of the destruction of 20-25 buildings and significant damage to cemeteries, suggesting that shaking was stronger in Santa Rosa than in San Francisco (Boatwright and Bundock, 2005). Other nearby cities in the Santa Rosa Plain, such as Petaluma (MM 7-8), Cotati (MM 7-8), and Sebastopol (MM9) were also significantly damaged in the earthquake. In the Sonoma Valley shaking is inferred to be MM 7-8 in Glen Ellen and MM 8 in Sonoma. Reports of damage in Napa Valley suggest shaking intensities around MM 8 in Napa from reports of toppled chimneys and cracked brick buildings, and MM 7-8 shaking occurring in the city of Yountville to the north (Boatwright and Bundock, 2005).

Two earthquakes larger than magnitude 5 have occurred since the implementation of modern instrumentation. An M_L 5.6 earthquake that was followed an hour and a half later by an M_L 5.7 earthquake in 1969 again damaged Santa Rosa. Shaking intensities of VII and VIII were felt in the city. Damage was estimated at $8.35 million in Santa Rosa and one person was killed (Toppozada, 2002) with 15 people injured (Wong and Bott, 1995). Many old brick and wood-frame buildings were irreparably damaged (Toppozada, 2002) which is surprising given the magnitude of the events. It is possible that a southern extension of the Healdsburg fault was the source of the earthquake, although the complex fault structure around Santa Rosa where the Rodgers Creek has a right step over to the Healdsburg and Maacama fault zones in the north has made definitive characterization of the 1969 earthquake source impossible (Wong and Bott, 1995). An M_L 5.2 west of Yountville on 3 September 2003 caused over $20 million in damage and injured 25 in the Napa Valley region (Federal Emergency Management Agency [FEMA], 2000). The amount of damage and the recorded accelerations were unexpectedly large given the magnitude of the earthquake (Langenheim et al., 2006). The earthquake appears to have occurred on an unnamed fault near the West Napa Fault as mapped by Jennings (1994), although the rupture location does coincide with mapping efforts by Fox (1983) and Clahan et al. (2004, 2005) on the West Napa fault, suggesting that its location may need to be revised (Langenheim et al., 2006).

3. Geological Setting

3a. Regional Geology

Basement rocks in the Northern San Francisco Bay region include those of the Mesozoic Great Valley Sequence and Franciscan complex (see Figure 1 for a map regional geology). Fragments of the Silinian formation are also present west of the San Andreas Fault. The Great Valley sequence is comprised of coherent depositional sequences of shale, sandstone, and conglomerate (Fox, 1983). The Franciscan Complex consists of tectonically and depositionally juxtaposed bodies of Graywacke, shale, and sandstone, mafic volcanic rocks (greenstone), mélange, broken formation, and ultramafic rocks. No depositional contact between the Great Valley sequence and the Franciscan complex is observed, although they are in contact across faults in several places (Fox, 1983). Some serpentine and serpentinized ultramafic rock is present in the study region as well.

The Tertiary Sonoma Volcanics are the only major igneous rocks in the region. They are comprised of a series of silicic basalt, andesite, and dacite flows, with interlayered ash and rhyolite flows in places and interbedded sandstone, gravel, and conglomerate. In regions north of our study, the Sonoma Volcanics are younger and are dominated by tuffaceous flows (Fox, 1983).

3b. Quaternary Geology

The age and type of near surface deposits can help infer their near surface velocity structure, which is a critical parameter in assessing site response. Quaternary sediments in the Santa Rosa Plain, Sonoma Valley, and Napa Valley include alluvial fan deposits, undifferentiated alluvium, basin deposits, and stream terrace deposits of various ages from the late Pleistocene to present (Figure 2) (Witter et al., 2006). San Francisco Bay

Muds are found along San Pablo Bay at the southern edge of our study area. Other Late Tertiary and/or early Quaternary sediments are present in the Santa Rosa Plain, generally comprised of gravel, sand, silt, and occasionally clay and minor tuff. West of Sebastopol, marine sands comprise the surface geology (Fox, 1983). Older Tertiary sediments made up of gravel, sand, silt, and clay and minor tuff are present near Petaluma (Fox, 1983). Detailed maps of quaternary geology can help explain differences in local amplifications that may be due to near surface sediments.

3c. Fault Structure

The fault structure in the region is dominated by the N-NW trending right-lateral strike slip faults of the Rodgers Creek-Healdsburg fault system, and Bennett-Valley Maacama fault system, which bound the eastern edge of the Santa Rosa Plain, and the West Napa fault, and the Concord-Green Valley fault system which bound the Napa Valley. These faults, as well as the Tolay and Carneros faults, all offset Miocene or younger strata in the Northern San Francisco Bay region (Fox, 1983). These strike-slip structures are all related to deformation along the San Andreas Fault, just west of our study area. The Rodgers Creek Fault may be connected beneath San Pablo Bay to the Hayward Fault in the south.

Active NW trending fold and thrust belts are disrupted by these strike slip systems. In particular, the Trenton Fault, about 10 km north of Sebastapol and striking 70°-75° N with a dip of about 17° NNE (Fox, 1983), appears to strongly influence basin structure near Santa Rosa. Thrust faults clearly influence regional topography and basin structure in the region (Mcloughlin et al., 2005).

3d. Basin Structure

The major cities of the Northern San Francisco Bay region sit above active depositional basins. As it is well known that basin depth, basin shape, and near surface geology play significant roles in amplifying seismic waves, it is a primary focus of this study to analyze the role of these two factors in the site response of the region. Sedimentary basins can amplify seismic waves by decreasing seismic impedance within the basin sediments relative to the surrounding rock (Tucker and King, 1984; Singh et al., 1988). Low-velocity rocks in sedimentary basins can also trap seismic waves, which can then be amplified by constructive interference (Trifunac, 1971; Harmsen and Harding, 1981; Lee and Langston, 1983; Graves et al., 1998; Frankel et al., 2001). These studies show the certain geometries and material properties can lead to the formation of standing waves and more complex patterns with high amplifications at the edges and middle of a basin (Fletcher et al., 2003). Given the highly localized damage observed historically in the Santa Rosa area, basin effects may be playing strong role in locally focusing and amplifying seismic waves.

Langenheim et al. (2006) have modeled the basin structure of the Northern San Francisco Bay region by compiling isostatic residual gravity data from several prior studies as well as their own data (Figure 3). The gravity data is a proxy for density that can help define lithologic contacts, provided there is sufficient density contrast between the rock units. With increasing depth of burial and age, the densities of the sedimentary basin fill may become indistinguishable from those of basement rocks (Langenheim et al, 2006). Further complicating basin modeling are the tertiary volcanic rocks present in the

region, which are characterized by a wide range in densities, but are on average less dense than the Mesozoic basement rocks (Langenheim et al., 2006). Results from the Napa Valley show two main sub-basins separated by a shallow ridge near Yountville. Deposits in the northern basin are may be as thick as 5km, although these could be high if the density contrast is lower than estimated. Beneath Napa, sedimentary fill may be as thick as 2 km. The Santa Rosa Plain is underlain by two main basins of 2-3 km thickness, the Windsor and the Cotati. A ridge separates the two basins near the city of Santa Rosa, believed to be related to the Trenton Thrust Fault (McPhee et al., 2005). A smaller pull-apart basin is formed to the east of Santa Rosa, likely as the result of a 5km wide step that connects the Rodgers Creek- Healdsburg Fault to the Maacama Fault (Langenheim et al., 2006b). The Sonoma Valley also appears to be underlain by two 1-3 km deep basins, with a shallow bedrock ridge near the two of Glen Ellen (Langenheim et al., 2005).

4. Data

4a. Seismic Data

Nineteen three-channel recorders were deployed in the northern San Francisco Bay Area with local dense arrays running across the cities of Napa (5 sites) and Santa Rosa (6 sites). Instrumentation was placed between December, 2003 and 2005. Stations were, for the most part, situated on alluvium. Stations were a mix of broadband (.03-50 Hz) 40T instruments (loaned by PASSCAL) and intermediate period (1 Hz) L4 instruments owned by the USGS. Concrete pads were placed for each sensor set to ensure that the horizontal components were stable. All of the recorders were three-

channel, 24-bit Ref-Tek 72a-07s. Each incorporated a GPS receiver which synchronized the internal clocks. The recorders were run in triggered mode at 200 samples per sec/channel. The dense arrays across the cities of Napa and Santa Rosa also had three additional channels for Kinemeterics "episensor" accelerometers. The Napa and Santa Rosa arrays were laid out in close spacing to provide better estimation of local amplification in these highly populated areas.

Local earthquakes were recorded from January, 2004, until September, 2007. Time windows were placed around background noise, P-wave arrivals, P-wave coda, and S-wave arrivals for events recorded by several seismograms with low background noise to be used for inversion. Log-spaced velocity power spectra were then computed from these seismograms, showing signal to noise over .01 to 50 Hz. Data that showed strong signal to noise were selected for the inversion runs. The interpretable band of frequencies was also determined form the signal to noise output, and in this study P waves give strong signal between 1 and 10 Hz., and S waves give strong signal between 1 and 8 Hz., but are dominated by noise past either frequency limit.

Two datasets were ultimately used in this study: one for P and S waves limited to hypocentral distance of 55km, and another with hypocentral distance limited to 100km (Table 1). Compressional wave dataset P < 100km has 266 records from 33 events recorded at all 24 stations, and dataset P < 55km has 169 records from 29 events recorded at 22 stations (NOV and VAC are excluded). Shear wave dataset S < 100km has 153 records from 25 events recorded, and dataset P < 55km has 124 records from 24 events, both recorded at 22 stations (NOV and VAC again excluded). These datasets were used to analyze differences in the model types, as will be discussed in the method section.

Hypocentral depths and moment magnitudes for the events were obtained from the Northern California Seismic Network data collection. Depths range from 1km to 13km and magnitudes range from M_w 1.6 to M_w 4.4 (Figure 1).

4b. Seismic Cone Penetration Data

To constrain near surface shear wave velocities and remove an ambiguity in the inversion,, seismic cone penetration testing (SCPT) was done at three sites in the city of Santa Rosa and three sites in the city of Napa (see Table 2 for summary of results and Figure 3 for velocity profiles). We used the average velocity above the deepest data point for rescaling site response. *Vs* 30m projections are shown in table 2, but are not used in this study. Shear wave velocities are faster near Santa Rosa, giving stations SAR and MAG NEHRP class C site classifications. Although station HEA has classification D, the velocity at maximum cone penetration is 281.3 m/s, consistent with velocities at SAR and MAG at that depth. Velocities in Napa were slower, with stations CAR, MDE, and VHD all falling within NEHRP class D.

4c. Suspension Log Data

Suspension Logging was used to constrain compressional velocities near Santa Rosa. Velocity profiles are shown in Figure 4. Although there is much variability in the velocities, the average velocities are very similar throughout. We used an average velocity of 1817 m/s at 100m depth of both velocity logs for geotechnical constraint in the inversion.

5. Method

We utilize the inversion scheme described in detail in Boatwright et al., (1991) and based on work by Andrews (1986). The method will only be summarized below. We invert seismograms to determine source, site, and propagation characteristics to determine site response at the seismic recording stations. The inversion scheme fits the logarithms of seismic body-wave spectra to the Brune source model (1970, 1971) with an ω^{-2} slope at high frequencies conditioned by geometric spreading, anelastic attenuation, mid-crustal attenuation. Residuals from this step are projected onto the set of sources and sites. These two steps are iterated until the square of the residuals is minimized. Finally, geotechnical data is used to rescale the estimated site response spectra to the equivalent quarter wavelength frequency determined from near-surface velocity data.

The inversion models attenuation caused by geometrical spreading, mid-crustal geology, and near-surface geology. Mid-crustal attenuation is defined by Q. In the original inversion, which we will refer to as tertio, a frequency independent average mid-crustal Q is determined. Falloff from geometrical spreading is modeled by r^{-1}. In this study, we also use a modified version of Boatwright et al.'s (1991) original inversion technique that solves for frequency dependent mid-crustal attenuation and utilizes a different model for falloff due to geometrical spreading that better models earthquakes with large hypocentral distances, which we will refer to as tertio(*f*). Determening a frequency dependent Q ensures that the average mid-crustal attenuation will not be characterized by attenuation of a dominant frequency as can occur when estimating a frequency independent Q. The modified inversion technique estimates frequency dependent mid-crutal Q by determining Q_0 in the equation $Q(f) = Q_0 f^{0.6}$ and models

13

falloff from geometrical spreading as r^{-1} for $r < 30$ km and $r^{-0.7}$ for $r > 30$ km. Both

inversion techniques estimate the near surface attenuation parameter t^*. We utilize

datasets for P and S waves with hypocentral radius limits of 55 km and 100 km for

comparison between the two models. We invert from 0.5 to 30.0 hz. for the P-wave

datasets and from 0.5 to 25.0 hz. for the S-wave datasets, beyond the interpretable

frequency range, to ensure that the inversion accurately picks corner frequencies.

Comparisons of inversion results from runs at lower frequency bands (e.g. 0.5 to 15.0 or

20.0 hz.) show that corner frequencies are stable for smaller corner frequencies ($f_c < 10$

hz.) with increasing inversion limits, with larger corner frequencies ($f_c > 10$ hz.)

becoming better determined.

6. Results

6a. Regional Results

Results from the inversions are summarized in Table 3. Average mid-crustal Q

and average t^* estimates vary between datasets, although the most stable results are

obtained for dataset P < 100km and S < 55km for both model Tertio and Tertio(f). Final

data variance is in comparison to the initial data variance, and is comparable for all

inversion runs. The mid-crustal Q of 739 obtained from the P <100km inversion is

similar to Q estimates from the San Francisco Peninsula of 790, although their S-wave Q

estimate of 830 is higher than the preferred estimate of 542 obtained in this study from

dataset S < 55km (Fletcher and Boatwright, 1991). Estimates of Q_0 are very similar for

P < 100km (136.3 +/- 0.4) and S < 55km (144.9 +/- 2.9).

14

Unreasonably low estimates of Q and physically impossible negative values for $t*$ are obtained for inversion of compressional waves with r < 55km. Estimates of Q and Q_0 for shear waves with r < 100 km are more than double the estimates for r < 50km. This may be due to sampling of higher velocity crust at greater depths for the r < 100km dataset, although it is unlikely that this should produce such a marked contrast. The wide range of $t*$ and Q values obtained is consistent with limitations in constraining corner frequency (f_c) discussed Fletcher and Boatwright (1991) for the effects of changing bandwidth on inversion parameters. Field and Jacob (1995) also note the wide range of permissible values that can be obtained when fitting f_c, $t*$, and Q to spectra, and note this can be beneficial since the actual values of each parameter need not be obtained so long as the pair of values together is correct. The interdependency of the variables means that the site response spectra should be unaffected by variations within an individual parameter so long as the others change correspondingly. Our varied results obtained from limiting the hypocentral distance demonstrates that $t*$ and Q estimates are also distance sensitive, and that we can only constrain these parameters to a range of permissible values exists. It is possible that we are seeing an azimuthal effect as a result of biasing the data in the P and S < 100km datasets, since a high percentage of events are from the Geysers region. Even with this variability, site response spectra remain fairly similar (see FigS. 5,6,7,8), particularly between the preferred datasets, P < 100km and S < 55km.

Site specific response estimates at all stations for our preferred S wave dataset, S < 55km, will be discussed below by region. Response spectra for S waves at stations NOV and VAC was not calculable due to limited data.

6a. Santa Rosa Plain

Figure 6 shows site response estimates for stations in and around the Santa Rosa Plain with t^* estimates for the 2 datasets and 2 models. Stations SAR, HEA, and MAG, are constrained by shear wave velocities from SCPT testing. The quarter wavelength is plotted on the graphs, with the depth of the averaged velocity shown below.

Response from dataset S < 55km is moderate between 1 and 8 Hz. at stations HEA (ranging from 6 to above 10) and MAG (ranging from 4 to 10), closest to Downtown Santa Rosa. Peaks in response between 1 and 3 Hz. are notable at stations SAR and EME, and a peak between 5 and 10 Hz. is observed at station HEA. At SAR, the response peaks at over between 8 (tertio) and 10 (tertio(*f*) at 2 Hz. Maximum response at HEA is at 2 Hz. for tertio(*f*) and exceeds 10, with response approaching 10 at 3 Hz. for model tertio. These peaks may be related to the basin structure, and will be addressed further in the discussion section. Stations PAP and ROP show the lowest site responses in the area.

6b. Sonoma Valley

Figure 7 shows estimated site response spectra for stations in the Sonoma Valley. They exhibit high variability in response between models, more so than any of the other regions. Even with significant variability, however, stations OAK and RAV exhibit similar spectral shapes between models, and provide sound results. Station IEW, however, shows pronounced variability between model results, and is not robust enough for firm conclusions. For the S < 55km dataset, response for models tertio and tertio(*f*) at

16

stations OAK and IEW are separated by at least a magnitude of 5 in estimated response at 3 Hz., with similar variability throughout the range of 1 to 8 Hz. Station RAV is better behaved, with separations of only 1 or 2 between the models. While response is moderate (ranging from 0 to 5) at RAV between 1 and 8 Hz., responses from model tertio(*f*) exceed 10 for both stations OAK and IEW. Tertio model results do not exceed 10 across that frequency band, and for station IEW, range between moderate values of 4 and 6.

6c. Napa Valley

The Napa Valley exhibits very strong site response, with stations YOU, VHD, and MDE showing amplifications between 10 and 20 between 1 and 8 Hz (Figure 8). The estimated amplifications exceed the quarter frequency estimates from SCPT velocities at stations VHD and MDE, however, suggesting that the response estimates may be high. Station CAR has a maximum response of 10 at about 3 Hz. and is the best fit to the quarter frequency of S-wave velocity of the three SCPT sites in Napa. Station HOT, which sits on Tertiary age rock, shows low site response, between 0 and 2 from 1 to 8 Hz., and provides a reference confirming the high relative amplification observed at the other Napa Stations. Station KRE sits on early to late Pleistocene undifferentiated alluvium, and exhibits about half the site response of adjacent stations VHD, MDE, and CAR. The spectra at stations in the Napa Valley are much more uniform than those in the Santa Rosa Plain, and aside from a small peak in amplitude around 3 Hz. at station CAR, are quite level. This lack of resonance feature may suggest that the near surface

geology is playing a bigger role than basin structure in amplifying seismic waves, as will be discussed in the conclusions.

6d. San Pablo Bay Area

Site response is unsurprizingly very high at our two stations along San Pablo Bay (Figure 9). Station SPT, which is situated on Quaternary San Francisco Bay Muds, has varied response between the models, but is above 10 for all models and datasets except for one minimum at 5 Hz. for model tertio(*f*). Response for dataset S < 55km approaches 20 at 2 Hz. for model tertio(*f*) and at 4 Hz. for model tertio. Response at station MAR, which is situated on artificial fill, is quite variable with strong attenuation 5 Hz. and response as low as 2 for model tertio(*f*), but peaks from 2-3 Hz. with amplifications approaching 9.

7. Discussion

Peaks in frequency at stations EME, SAR, and perhaps HEA in the Santa Rosa Plain occur at stations near the edge of basins, with approximately 1-1.25 km of basin depth beneath them (Figure 3). SAR sits at the southeastern extent of the Windsor Basin, and EME sits and the northwestern edge of the Cotati Basin. These suggest some resonance of the basin, and perhaps also refraction of waves in the slower sediments that is resulting in constructive interference.

Depth to basement does not seem to play a strong role in determining shaking in the Santa Rosa Plain, however, as station ROP, which sits above 1.25-1.5 km of basin, has lower site response than station MAG, which sits above less than 0.25 km of basin.

The younger and presumably slower velocity, near-surface Holocene alluvial fan deposits at station MAG may explain the strong response. Faster Late Pleistocene age alluvium at station EME may also explain why that station exhibits lower response.

Basin depth appears to strongly correlate with shaking in the Napa Valley, with strong response at stations MDE and CAR above deeper basin, and correspondingly lower response at stations KRE and HOT. Strong response is also observed at station VHD and YOU, however, which are both on the edges of basins. Aside from perhaps station CAR, however, no peaks in the spectra suggesting resonance are observed. Quaternary geology shows some correlation with response, with high response stations MDE and CAR sitting above Holocene alluvium, and station KRE, which sits above early to late Pleistocene alluvial deposits, shows lower response. Station VHD, however, which is on top of Holocene to latest Pleistocene alluvium, shows amplifications nearly as high as MDE and CAR. This discrepancy suggests that sites above deep basins and along basin edges are most prone to amplification.

8. Conclusions

Site Response in the Northern San Francisco Bay area is estimated to be high in many areas, confirming high historical shaking intensities. Shaking appears to be high nearly as high along the edges of basins in the Santa Rosa Plain and Napa Valley as it is above deeper parts of the basin. Near-surface geology appears to play a stronger role in amplifying waves in the Napa Valley than it does in Santa Rosa, but high amplifications are also observed at sites along the edges of basins here as well.

Acknowledgments

References

Andrews, D. J. (1986). Objective determination of source parameters and similarity of earthquakes of different size, in *Earthquake Source Mechanics*, S. Das, J. Boatwright, and C. H. Scholz (Editors), American Geophysical Union, Washington, D.C., 259–268.

Boatwright, J. and H. Bundock (2005). Modified Mercalli Intensity Maps for the 1906 San Francisco Earthquake Plotted in ShakeMap Format. *U.S. Geol. Surv. Open-File Rept. 05-1135*, http://pubs.usgs.gov/of/2005/1135/ (Last accessed January 2007).

Boatwright, J., J. B. Fletcher, and T. E. Fumal (1991). A general inversion scheme for source, site, and propagation characteristics using multiply recorded sets of moderate-size earthquakes, *Bull. Seism. Soc. Am.* **81,** 1754–1782.

Brune, J. N. (1970). Tectonic stress and spectra of seismic shear waves from earthquakes, *J. Geophys. Res.* **75,** 4997–5009.

Brune, J. N. (1971). Correction, *J. Geophys. Res.* **76,** 5002.

Clahan, K. B., D. L. Wagner, S. P. Bezore, J. M. Sowers, and R. C. Witter (2005). Geologic map of the Rutherford 7.5_ quadrangle, Napa County, California, California Geological Survey Preliminary Geologic Map, www.conservation.ca.gov/cgs/rghm/rgm/preliminary_geologic_maps.htm (Last accessed January 2007).

Clahan, K. B., D. L. Wagner, G. L. Saucedo, C. E. Randolph-Loar, and J. M. Sowers (2004). Geologic map of the Napa 7.5_ quadrangle, Napa County, California, California Geological Survey Preliminary Geologic Map, www.conservation.ca.gov/cgs/rghm/rgm/preliminary_geologic_maps.htm (Last accessed January 2007).

Federal Emergency Management Agency (FEMA) (2000). California Earthquake Declared September 14, 2000, www.fema.gov/news/event.fema?id=275 (Last accessed January 2007).

Fox, K. F., Jr. (1983). Tectonic setting of late miocene, pliocene, and pleistocene rocks in part of the coast ranges north of San Francisco, California, *U.S. Geol. Surv. Profess. Pap. 1239*, 33pp.

Field, E. H., & Jacob, K. H. (1995). A comparison and test of various site-response estimation techniques, including three that are not reference-site dependent. *Bulletin of the Seismological Society of America, 85*(4), 1127-1143. Retrieved February 2, 2007, from Earthquake Engineering Abstracts database.

Fletcher, J. P. B., Boatwright, J. L., & Lindh, A. G. (2003). Wave propagation and site response in the santa clara valley. *Bulletin of the Seismological Society of America, 93*(1), 480-500. Retrieved February 2, 2007, from GeoRef database.

Fletcher, J. B., and J. Boatwright (1991). Source parameters of Loma Prieta aftershocks and wave propagation characteristics along the San Francisco Peninsula from a joint inversion of digital seismograms, *Bull. Seism. Soc. Am.* **81,** 1783–1812.

Frankel, A., D. Carver, E. Cranswick, T. Brice, R. Sell, and S. Hanson (2001). Observations of basin ground motions from a dense seismic array in San Jose, California, *Bull. Seism. Soc. Am.* **91,** 1–12.

Graves, R. W., A. Pitarka, and P. G. Somerville (1998). Ground-motion amplification in the Santa Monica area: Effects of shallow basin-edge structure, *Bull. Seism. Soc. Am.* **88,** 1224–1242.

Graymer, R. W., Bryant, W., McCabe, C. A., Hecker, S., & Prentice, C. S. (2006). *Map of quaternary-active faults in the san francisco bay region* (16 Structural geology; 19 Seismology No. SIM-2919). United States (USA): February 2, 2007, from GeoRef database.

Graymer, R. W., Moring, B. C., Saucedo, G. J., Wentworth, C. M., Brabb, E. E., & Knudsen, K. L. (2006b). *Geologic map of the san francisco bay region* (13, Areal geology No. SIM-2918). United States (USA): February 2, 2007, from GeoRef databaseHarmsen, S., and S. Harding (1981). Surface motion over a sedimentary valley for incident plane P and SV waves, *Bull. Seism. Soc. Am.* **71,** 655–670.

Jennings, C.W. (1994). Fault Activity map of California and adjacent areas. Calif. Div. Mines Geol. Geol. Data Map 6, scale 1:750,000.

Langenheim, V.E., R.W. Graymer, and R.C. Jachens (2006). Geophysical Setting of the 2000 M_L 5.2 Yountville, California, Earthquake: Implications for Seismic Hazard in Napa Valley, California.

Langenheim, V., McLaughlin, R., & Jachens, R. (2006b). Insights into the evolution of faulting along the Rodgers Creek-Healdsburg-Maacama fault zones, northern California, as revealed by gravity and magnetic data. *100th anniversary earthquake conference. 2006; 100th anniversary earthquake conference including the 8th U.S. national conference on earthquake engineering (8NCEE), the SSA centennial meeting, and the OES disaster resistant California conference,* San Francisco, CA.

Langenheim, V. E., Wagner, D. L., Farrar, C. D., & Sweetkind, D. (2005). Structure of sonoma valley, california revealed by geologic and geophysical mapping; a fault-bend basin within the rodgers creek and bennett valley fault zones?; geological society of america, cordilleran section, 101st annual meeting; american

association of petroleum geologists, pacific section, 80th annual meeting. *Abstracts with Programs - Geological Society of America, 37*(4) 84.

Lawson, A. C. (1908). The california earthquake of april 18, 1906. *254 pp,* Retrieved February 2, 2007, from GeoRef database.

Lee, J.-J., and C. A. Langston (1983). Wave propagation in a three-dimensional circular basin, *Bull. Seism. Soc. Am.* **73,** 1637–1653.

McLaughlin, R. J., Sarna-Wojcicki, A. M., Fleck, R. J., Langenheim, V. E., McPhee, D. K., & Graymer, R. W. et al. (2005). Late cenozoic volcanism and basin formation within a tectonic setting transitional from subduction to dextral strike-slip, northern san francisco bay region, california; geological society of america, cordilleran section, 101st annual meeting; american association of petroleum geologists, pacific section, 80th annual meeting. *Abstracts with Programs - Geological Society of America, 37*(4), 83. Retrieved February 2, 2007, from GeoRef database.

McPhee, D. K., Langenheim, V. E., Jachens, R. C., McLaughlin, R. J., & Roberts, C. W. (2005). Basin structure beneath the Santa Rosa Plain, northern California, and its possible influence on damage patterns from the 1906 and 1969 earthquakes; geological society of america, cordilleran section, 101st annual meeting; american association of petroleum geologists, pacific section, 80th annual meeting. *Abstracts with Programs - Geological Society of America, 37*(4) 84.

Petersen, M.D. W.A. Bryant, C.H. Cramer, T. Cao, and M. Reichle (1996). Probabilistic Seismic Hazard Assessment for the State of California. *U.S. Geol. Surv. Open-File Rept. 03-214*, http://www.consrv.ca.gov/cgs/rghm/psha/ofr9608/index.htm (Last accessed January 2007).

Rowshandel B., M. Reichle, C. Wills, T. Cao, M. Petersen, D. Branum, and J. Davis (2006). Estimation of Future Earthquake Losses in California. *California Geological Survey*, ftp://ftp.consrv.ca.gov/pub/dmg/rgmp/CA-Loss-Paper.pdf (Last accessed January 2007).

Singh, S. K., E. Mena, and R. Castro (1988). Some aspects of source characteristics of the 19 September 1985 Michoacan earthquake and ground motion amplification in and near Mexico City from strong motion data, *Bull. Seism. Soc. Am.* **78,** 451–477.

Toppozada, T. R. (2002). San andreas fault zone, california: M greater than or equal to 5.5 earthquake history. *Bull. Seism. Soc. Am.* **92**, 2555-2601.

Toppozada, T. R. (1992). 1898 "mare island" earthquake at the southern end of the rodgers creek fault. *Proceedings of the second conference on earthquake hazards in the eastern san francisco bay area; proceedings of the second conference on*

earthquake hazards in the eastern san francisco bay area, 385-392. Retrieved February 2, 2007, from Earthquake Engineering Abstracts database.

Trifunac, M. D. (1971). Surface motion of a semi-cylindrical alluvial valley for incident SH waves, *Bull. Seism. Soc. Am.* **61,** 1755–1770.

Tucker, B. E., and J. L. King (1984). Observed variations of earthquake motion across a sediment-filled valley, *Bull. Seism. Soc. Am.* **74,** 153–165.

Wong, I. G., & Bott, J. D. J. (1995). A new look back at the 1969 santa rosa, california, earthquakes. *Bulletin of the Seismological Society of America, 85*(1), 334-341. Retrieved February 2, 2007, from GeoRef database.

Working Group on California Earthquake Probabilities (2003). Earthquake Probabilities in the San Francisco Bay Region: 2002–2031. *U.S. Geol. Surv. Open-File Rept. 03-214*, http://pubs.usgs.gov/of/2003/of03-214/ (Last accessed January 2007).

Table 1: Earthquakes Used for Inversion

Event ID	Date	Latitude	Longitude	Depth (km)	Magnitude	P < 100km	P < 55km	S < 100km	S < 55km
0472024	2/16/2004	38.3292 N	122.5767 W	7.23	3.03	X	X	X	X
2060426	7/24/2004	38.8105 N	122.8097 W	3.63	2.89	X		X	
2511057	9/7/2004	38.7608 N	122.7163 W	2.18	3.06	X	X	X	X
2521715	9/8/2004	38.3998 N	122.4373 W	10.75	2.92	X	X	X	X
2980247	10/24/2004	38.7708 N	122.7417 W	0.91	3.41	X	X	X	X
3031802	10/29/2004	38.8177 N	122.7912 W	3.38	3.81	X	X	X	X
1621224	6/11/2005	38.4075 N	122.2122 W	9.27	2.59	X	X	X	X
1621242	6/11/2005	38.4120 N	122.2033 W	10.46	2.78	X	X	X	X
1911537	7/10/2005	38.5267 N	122.4343 W	11.21	2.43	X	X	X	X
1920804	7/11/2005	38.3320 N	122.3982 W	10.69	1.60	X	X		X
2371110	8/25/2005	38.3620 N	122.1850 W	9.87	3.16	X	X	X	X
2410236	8/29/2005	38.8172 N	122.8215 W	2.99	3.10	X			
2530203	9/10/2005	38.5252 N	122.2972 W	9.30	2.53	X	X	X	X
2550636	9/12/2005	38.5225 N	122.3118 W	8.32	2.19	X	X	X	X
2671125	9/24/2005	37.8302 N	122.2213 W	5.43	3.22	X			
2820901	10/9/2005	37.8520 N	122.2425 W	6.14	2.66	X	X		
3180900	11/14/2005	38.7940 N	122.8020 W	4.08	2.89	X	X	X	X
3210855	11/17/2005	38.8138 N	122.7835 W	2.42	3.87	X	X	X	
3501821	12/16/2005	38.0032 N	122.2530 W	5.80	3.37	X	X	X	X
3541435	12/20/2005	38.4515 N	122.6402 W	10.41	2.62	X	X	X	X
0060436	1/6/2006	38.3788 N	122.2077 W	7.45	2.46	X	X	X	X
0081015	1/8/2006	38.8320 N	122.7997 W	2.10	2.90	X	X		
0310917	1/31/2006	38.8287 N	122.7915 W	2.15	3.08	X	X	X	
0802141	3/21/2006	37.8093 N	122.0710 W	12.94	3.70	X		X	
0821017	3/23/2006	38.7690 N	122.7368 W	2.39	3.07	X	X	X	X
0860822	3/27/2006	38.4682 N	122.7443 W	8.61	2.14	X	X		
0970927	4/7/2006	38.7762 N	122.7452 W	2.11	3.05	X	X	X	X
1281053	5/8/2006	38.2457 N	122.1782 W	9.60	1.55	X	X		
1321037	5/12/2006	38.8160 N	122.8168 W	2.89	4.39	X	X	X	X
1480107	5/28/2006	38.4795 N	122.7120 W	6.03	3.05	X	X		X
1700555	6/19/2006	38.7890 N	122.7762 W	4.58	3.15	X	X	X	X
2150308	8/3/2006	38.3635 N	122.5887 W	8.86	4.40	X	X	X	X
2201946	8/8/2006	38.4213 N	122.2428 W	7.66	2.87	X	X	X	X

Table 2: Stations and S-wave Velocities Used in Constraining Site Amplifications

Station Name	Latitude	Longitude	Max Depth (m)	Average measured Velocity (m/s)	Projected V_s 30m (m/s)	NEHRP Site Classification
CAR	38.3069 N	122.2922 W	19.5	248.8	313	D
MDE	38.3174 N	122.3087 W	15.7	218.5	333	D
VHD	38.3286 N	122.3336 W	15.7	236.2	357	D
HEA	38.4375 N	122.7373 W	18.5	281.3	314	D
SAR	38.4956 N	122.7438 W	18.5	277.3	405	C
MAG	38.4468 N	122.6812 W	12.8	281.6	476	C

## Table 3: Comparison of Regional Model Results

Dataset	Model	Frequency Limits (hz.)	Iterations	Variance	Non-ste specific t* (s)	Q
P < 100km	Tertio	0.5-30.0	5	1.32862 %	0.0049 +/- 0.0000	739.4 +/- 0.4
P < 100km	Tertio(*f*)	0.5-30.0	18	1.21884 %	0.0126 +/- 0.0002	136.3 +/- 0.6
P < 55km	Tertio	0.5-30.0	7	0.97150 %	-0.0173 +/- 0.0001	178.4 +/- 0.1
P < 55km	Tertio(*f*)	0.5-30.0	20	0.92229 %	-0.0063 +/- 0.0002	28.9 +/- 0.1
S < 100km	Tertio	0.5-25.0	5	0.75319 %	0.0263 +/- 0.0001	1162.1 +/- 1.1
S < 100km	Tertio(*f*)	0.5-25.0	25	0.71427 %	0.0427 +/- 0.0007	387.6 +/- 3.5
S < 55km	Tertio	0.5-25.0	6	0.68135 %	0.0075 +/- 0.0001	542.2 +/- 0.7
S < 55km	Tertio(*f*)	0.5-25.0	23	0.63833 %	0.0293 +/- 0.0018	144.9 +/- 2.9

Fig 2: Quaternary Geology*

Santa Rosa Plain
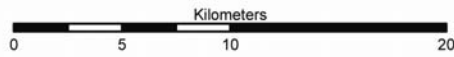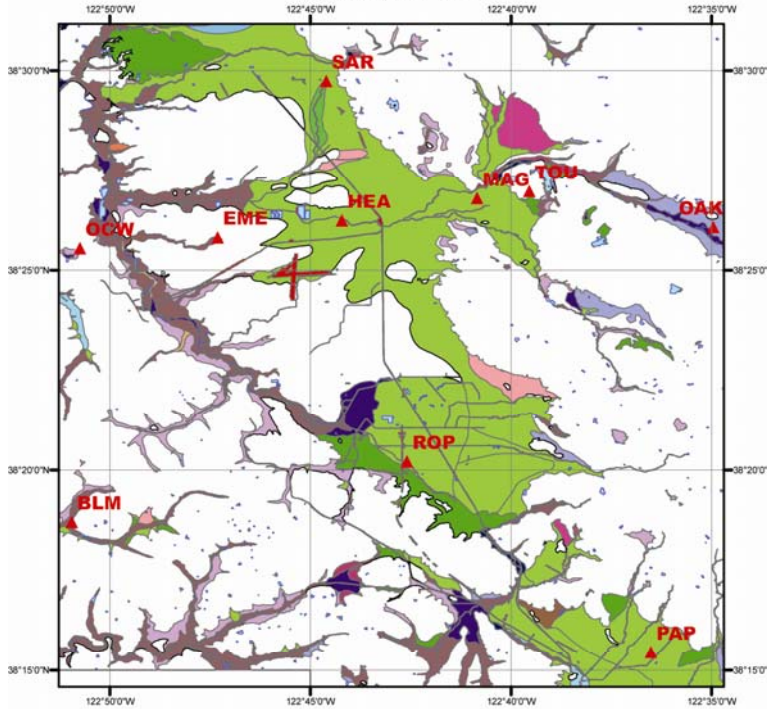
Napa Valley
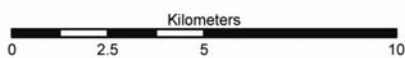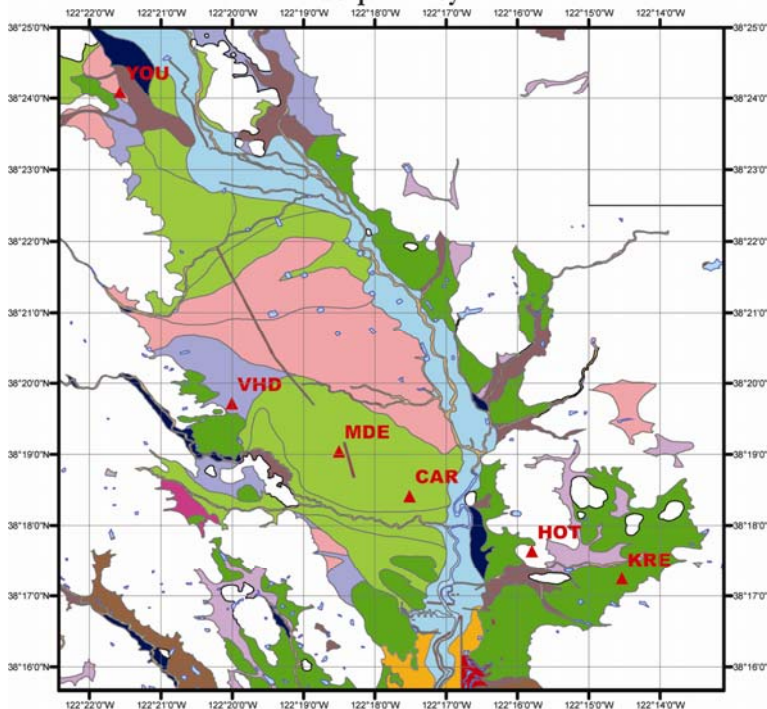
Map Units

▲ Stations

Modern

H2O	Water
Qhc	Stream channel deposits
a	Artificial fill

Latest Holocene

Qhly	Alluvial fan levee deposits
Qhty	Stream terrace deposits
Qhbs	Beach sand

Holocene

Qhds	Dune sand
Qhbm	San Francisco Bay mud
Qhed	Estuarine delta deposits
Qhb	Basin deposits
Qhf	Alluvial fan deposits
Qhl	Alluvial fan levee deposits
	Stream terrace deposits
Qha	Alluvium, undifferentiated

Holocene to latest Pleistocene

Qds	Dune sand
Qb	Basin deposits
Qf	Alluvial fan deposits
Qt	Stream terrace deposits
Qa	Alluvium, undifferentiated

Latest Pleistocene

Qpa	Alluvium, undifferentiated
Qpf	Alluvial fan deposits
Qpt	Stream terrace deposits

Pleistocene

Qmt	Marine terrace deposits
Qbt	Bay terrace deposits

Early to late Pleistocene

Qoa	Alluvial deposits, undifferentiated
Qof	Alluvial fan deposits
Qop	Pediment deposits
Qot	Stream terrace deposits

Pre-Quaternary

br	Pre-Quaternary deposits and bedrock

*Map data from Witter, R.C., et al. (2006)

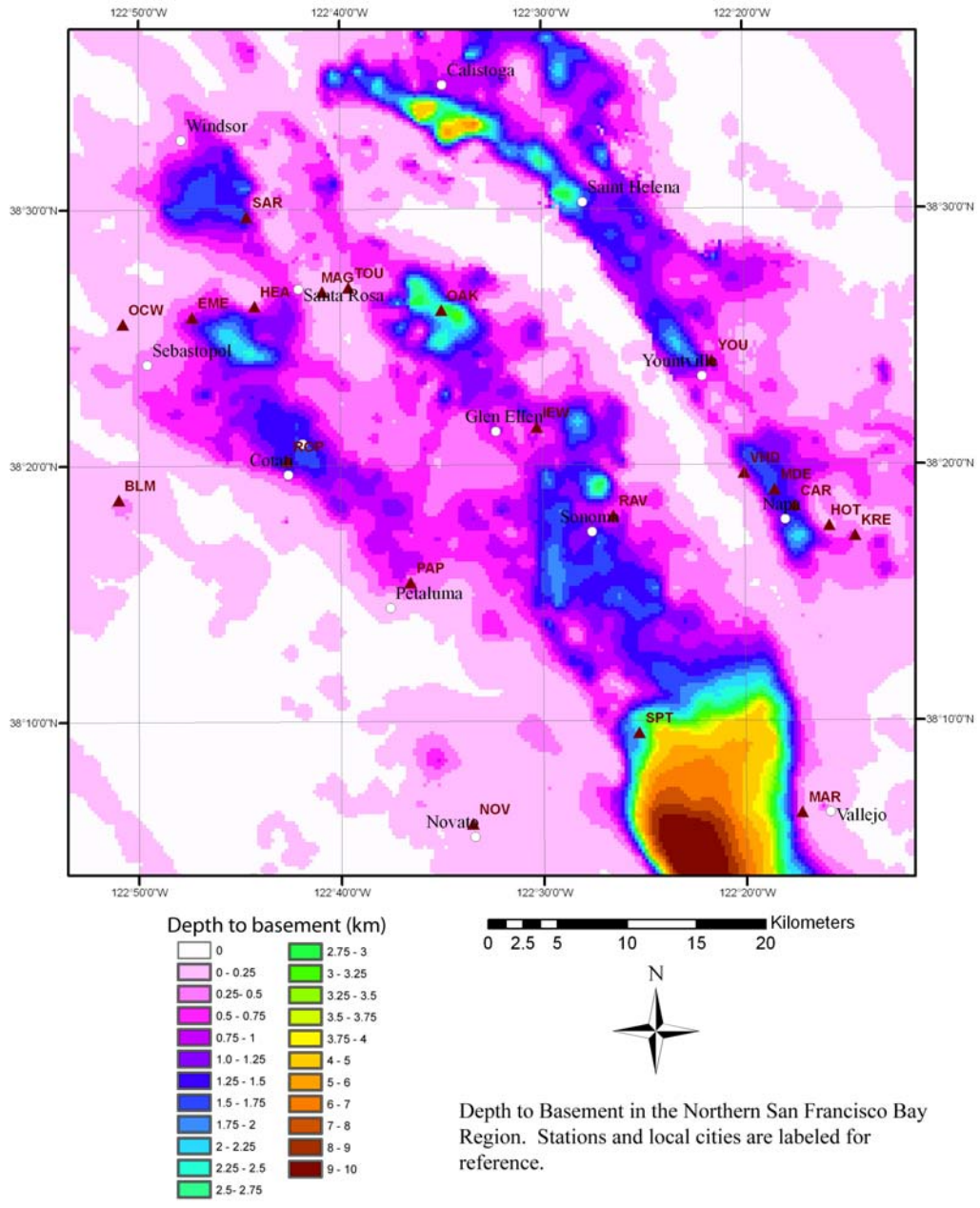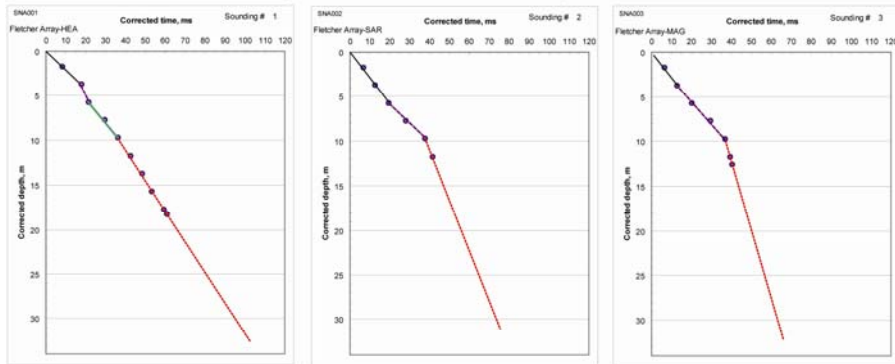# Figure 3: Basin Depth in Northern San Francisco Bay Region

Depth to basement (km)

0	2.75 - 3
0 - 0.25	3 - 3.25
0.25- 0.5	3.25 - 3.5
0.5 - 0.75	3.5 - 3.75
0.75 - 1	3.75 - 4
1.0 - 1.25	4 - 5
1.25 - 1.5	5 - 6
1.5 - 1.75	6 - 7
1.75 - 2	7 - 8
2 - 2.25	8 - 9
2.25 - 2.5	9 - 10
2.5- 2.75	

Depth to Basement in the Northern San Francisco Bay Region. Stations and local cities are labeled for reference.

Fig 4: Santa Rosa Shear Wave Velocity Profiles

Napa Shear Wave Velocity Profiles
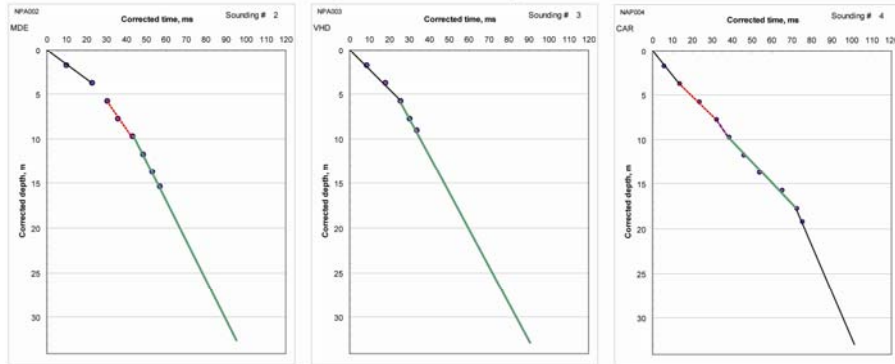
Figs. 3 and 4: Shear wave velocity profiles from seismic cone penetration testing at stations in the cities of Santa Rosa and Napa (station name at upper left, see Fig. 2 for location). The average velocity above the deepest data point at each station was used in rescaling site response.

30

Fig 5: Santa Rosa Compressional Velocity Profiles
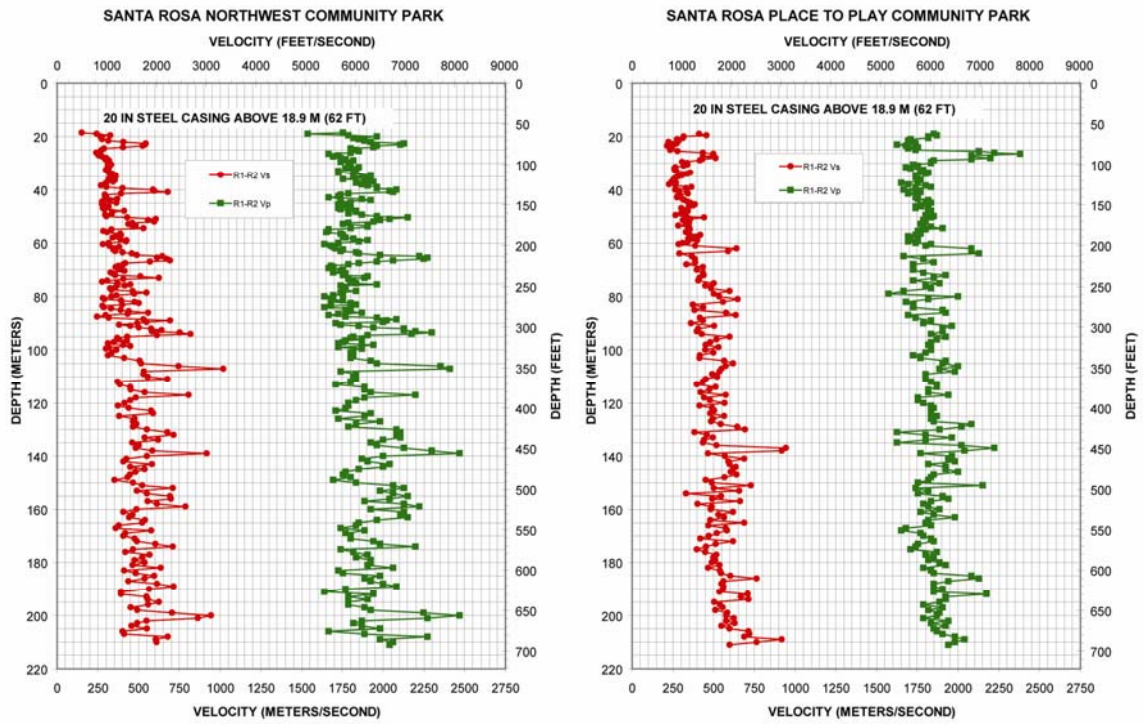
Fig. 4: Compressional wave velocity profiles from suspension log data in the city of Santa Rosa. The average velocity above 100 meters was used in rescaling site response at all stations in Santa Rosa.
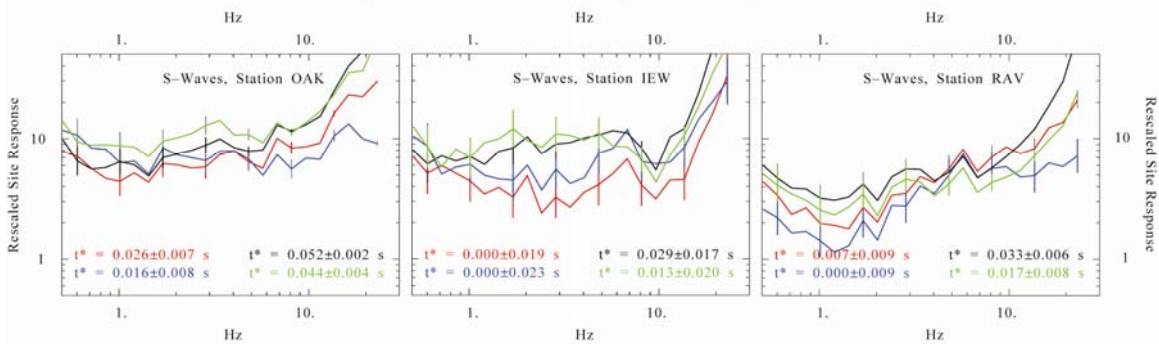
Figure 6: Santa Rosa Plain Site Response
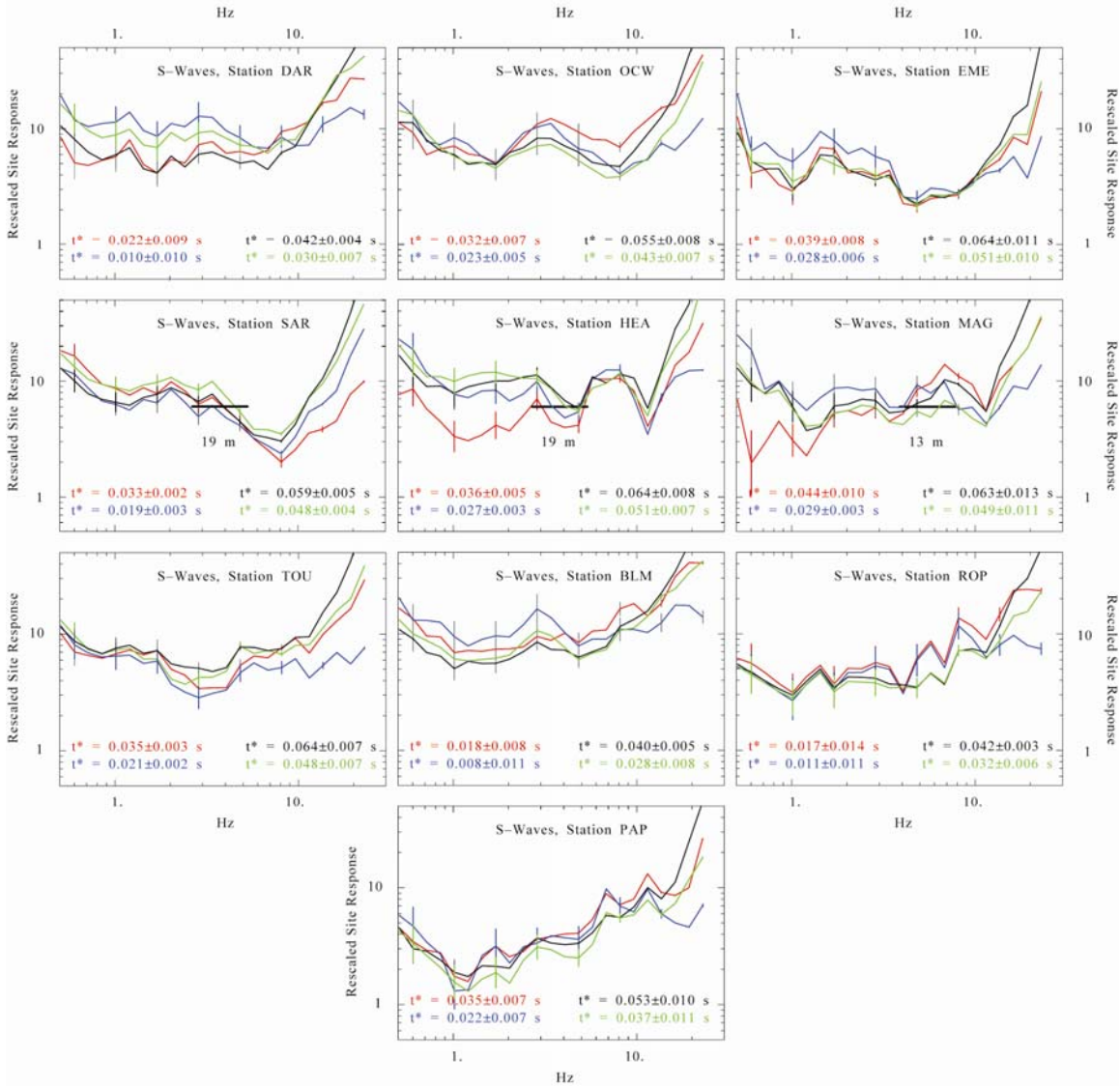
Figure 6: Site response spectra for the Santa Rosa Plain. Red lines show estimates for dataset S < 100km and model tertio. Blue lines show estimates for dataset S < 55km and model tertio. Black lines show estimates for dataset S < 100km and model tertio(*f*). Green lines show estimates for dataset S < 55km and model tertio(*f*). The preferred results are shown in green and blue.
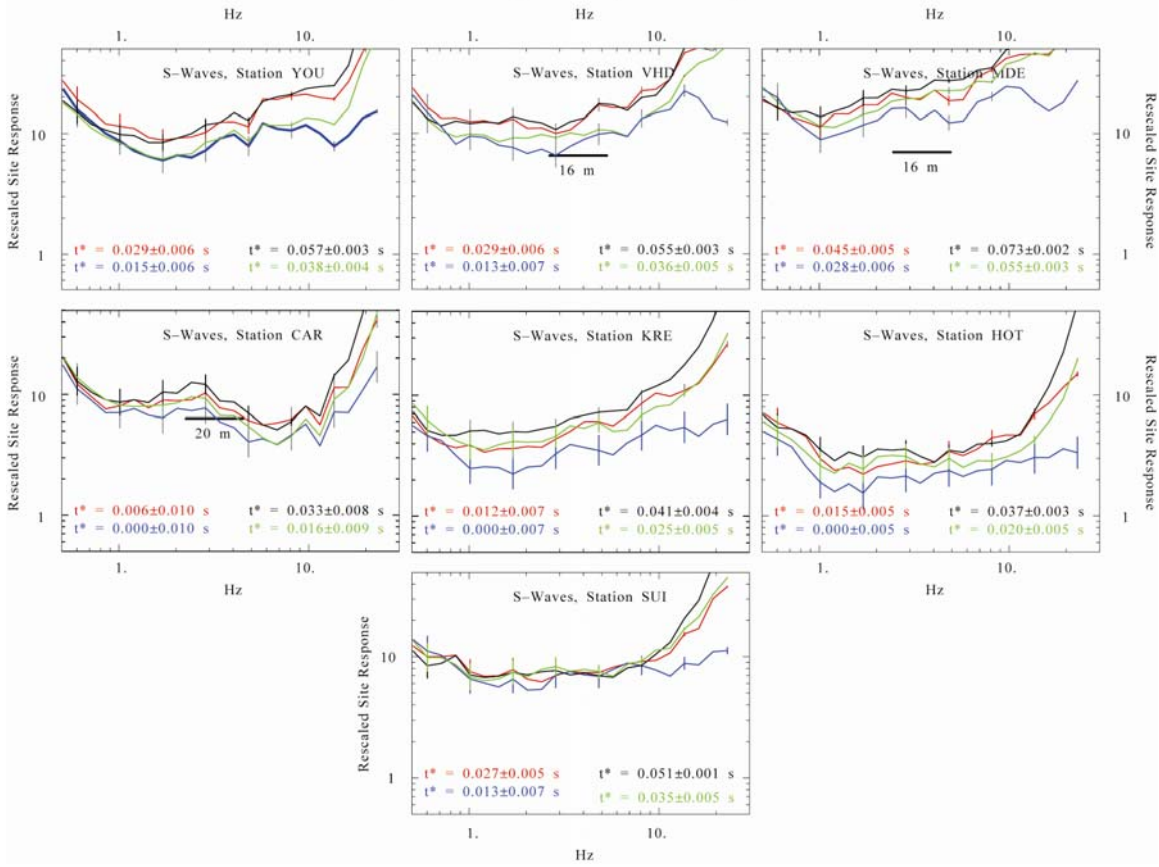
Figure 7: Site response spectra for the Sonoma valley. Red lines show estimates for dataset S < 100km and model tertio. Blue lines show estimates for dataset S < 55km and model tertio. Black lines show estimates for dataset S < 100km and model tertio(*f*). Green lines show estimates for dataset S < 55km and model tertio(*f*). The preferred results are shown in green and blue.

Figure 8: Napa Valley Site Response

Figure 8: Site response spectra for the Napa Valley. Red lines show estimates for dataset S < 100km and model tertio. Blue lines show estimates for dataset S < 55km and model tertio. Black lines show estimates for dataset S < 100km and model tertio(*f*). Green lines show estimates for dataset S < 55km and model tertio(*f*). The preferred results are shown in green and blue.

Figure 9: San Pablo Bay Area Site Response
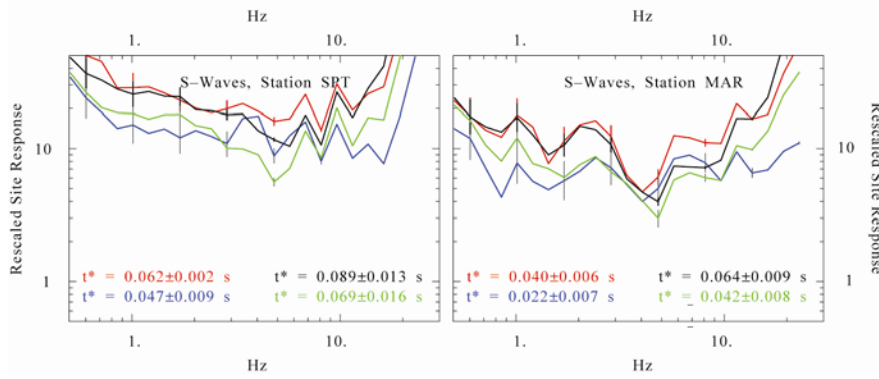

Figure 6: Site response spectra for the San Pablo Bay Area. Red lines show estimates for dataset S < 100km and model tertio. Blue lines show estimates for dataset S < 55km and model tertio. Black lines show estimates for dataset S < 100km and model tertio(*f*). Green lines show estimates for dataset S < 55km and model tertio(*f*). The preferred results are shown in green and blue.